

# Covariant description of kinetic freeze out through a finite time-like layer

E. Molnár<sup>1</sup>, L. P. Csernai<sup>1,2</sup>, V. K. Magas<sup>1,3</sup>, Zs. I. Lázár<sup>1,4</sup>, A. Nyíri<sup>1</sup> and K. Tamosiunas<sup>1</sup>

<sup>1</sup> *Section for Theoretical and Computational Physics,  
and Bergen Computational Physics Laboratory,  
BCCS-Unifob, University of Bergen,  
Allegaten 55, 5007 Bergen, Norway*

<sup>2</sup> *MTA-KFKI, Research Inst of Particle and Nuclear Physics,  
H-1525 Budapest 114, P.O.Box 49, Hungary*

<sup>3</sup> *Departamento de Física Teórica and IFIC Centro Mixto  
Universidad de Valencia-CSIC,  
Institutos de Investigación de Paterna*

*Apdo. correos 22085, 46071, Valencia, Spain*  
<sup>4</sup> *Department of Theoretical and Computational Physics,  
Faculty of Physics, Babeş-Bolyai University,  
Str. M. Kogălniceanu, nr. 1B,  
400084 Cluj-Napoca, Romania*

**Abstract:** The Freeze Out (FO) problem is addressed for a covariant FO probability and a finite Freeze Out layer with a time-like normal vector. The resulting post FO momentum distribution functions are presented and discussed. In general the post FO distributions are non-thermal, asymmetric distributions.

PACS numbers: 24.10.Nz, 25.75.-q

## I. INTRODUCTION

Freeze out (FO) is a term referring to the stage of expanding or exploding matter when its constituents (particles) loose contact, collisions cease, and local dynamical equilibrium is not maintained. We describe this phenomenon via the example of a relativistic heavy ion collision. In local equilibrium, the evolution of the system can be described by hydrodynamics, while at the end of the hydrodynamical description the matter freezes out. For  $p + p$  reactions this description was first proposed by Landau [1] in the early 1950's.

The hydrodynamical equations are expressions of conservations laws in the presence of continuity and local equilibrium. When the local equilibrium is significantly perturbed, the microscopic length and time scales become comparable to the characteristic macroscopic ones, the hydrodynamical approach breaks down. In the absence of collisions the momentum distribution of the particles *freezes out*, hence the name kinetic FO.

Starting from the first instant of the hydrodynamical expansion there are particles that leave the interacting system. As time passes the system becomes more dilute, the number of non-interacting particles increases until the whole system breaks up and expands freely without inter-particle collisions. This is the end of the freeze out stage, when the particle momentum is frozen out.

Let us assume the validity of hydrodynamical treatment up to a sharp FO hypersurface, at a constant freeze out temperature. All particle interactions will cease suddenly when reaching the FO temperature, this is a *sudden* FO process. Thus, the freeze out can be considered as a discontinuity, where the properties of matter change suddenly, across a hypersurface in space-time.

This strong assumption is the limiting case of a more realistic *gradual* FO process, where the FO description applies over a finite space-time domain, i.e. freeze out layer. Thus, the particles are formed and emitted at different "temperatures" gradually over the expansion volume. However, both descriptions share a common treatment as far as the conservation laws are concerned.

The properties of the matter are different on the two sides (Pre and Post) of the FO front, but the conservation of baryon charge, energy-momentum and the positive entropy change must hold, thus

$$[N^\mu d\sigma_\mu] = 0, \quad [T^{\mu\nu} d\sigma_\mu] = 0, \quad [S^\mu d\sigma_\mu] \geq 0, \quad (1)$$

where the Pre FO baryon and entropy currents and the energy-momentum tensor are  $N_0^\mu, S_0^\mu, T_0^{\mu\nu}$ , while the Post FO quantities are  $N^\mu, S^\mu, T^{\mu\nu}$ , and the square brackets denote the difference,  $[A] \equiv A - A_0$ .

As it was shown recently [2], the conservation laws are valid over any surface of discontinuity in relativistic flow. Physically we distinguish two types of hypersurfaces, one with a time-like normal vector ( $d\sigma_\mu d\sigma^\mu = 1$ ), and one with a space-like normal vector ( $d\sigma_\mu d\sigma^\mu = -1$ ). This is important when we calculate final particle spectra, since the widely used method by Cooper and Frye [3] gives a misleading result when it is applied over a FO hypersurface with a space-like normal vector. The solution for this conceptual problem was addressed in recent works [4, 5, 6, 7], resulting in a non-equilibrium cut-off post FO distribution, ensuring that all particles leave the surface only outwards:

$$f_{PostFO}(x, p; d\sigma^\mu) = f_{PostFO}(x, p) \Theta(p^\mu d\sigma_\mu), \quad (2)$$

where both distribution functions depend on particle density, temperature and flow velocity. If we take the

integral of the post FO distribution over the FO hypersurface together with eq. (2), we obtain the (Modified) Cooper-Frye formula:

$$E \frac{dN}{d^3p} = \int_S f_{PostFO}(x, p; d\sigma^\gamma) p^\mu d\sigma_\mu, \quad (3)$$

where the phase-space distribution of the frozen out particles is not known from the hydrodynamical model. Thus, it is our task to find the final momentum distribution, to use the correct parameters of the matter and evaluate the FO measurable on the post FO side.

The kinetic freeze out model over infinitely long space-like and time-like layer was discussed in many recent papers [6, 8, 9, 10]. This paper is partly based on the above mentioned works. A simple kinetic approach is presented in a covariant formalism for a finite time-like layer. The basic philosophy of this paper is similar to the recent paper [11], where the fully covariant treatment is presented for a finite space-like FO layer.

Below we will generalize the kinetic freeze out treatment for a finite time-like FO layer, and show that our approach can easily handle both space-like and time-like freeze out processes on the same fully covariant footing.

## II. FINITE DOMAIN KINETIC FREEZE OUT MODELS

To model the FO mechanism inside a finite space-time layer, we start with some basic assumptions, which can be easily understood following Fig. 1, and the conservation laws across the FO layer.

To begin with, we recall the kinetic definition of the particle four current of conserved charges:

$$N^\mu(x) = \int \frac{d^3p}{p^0} p^\mu f(x, p), \quad (4)$$

where the total number of particles crossing the FO surface in the  $d\sigma_\mu$  direction is:

$$N_S = \int_S N^\mu(x') d\sigma_\mu = \int_S d\sigma_\mu \int \frac{d^3p}{p^0} p^\mu f(x', p). \quad (5)$$

This expression is valid over any type of 3D time-like hypersurface, while the total number of particles between two parallel hypersurface elements, is

$$\begin{aligned} \Delta N_S &\equiv \int_{\Delta S_2} N^\mu(x') d\sigma_\mu - \int_{\Delta S_1} N^\mu(x') d\sigma_\mu \quad (6) \\ &= \int_{\Delta^4 x} ds^\mu d\sigma_\mu [\partial_\mu N^\mu(x')] \\ &= \int_{\Delta^4 x} d^4x \int d^3p \frac{p^\mu}{p^0} [\partial_\mu f(x', p)] = 0, \end{aligned}$$

where  $ds^\mu$  is the length element in the direction of freeze out,  $d\sigma_\mu \equiv d^3\sigma_\mu$  is the hypersurface element and

$ds^\mu d\sigma_\mu = d^4x$ . Thus, the conservation of the total number of particles requires

$$\partial_\mu N^\mu(x) = 0. \quad (7)$$

The freeze out of particles starts from the inside boundary of the FO layer,  $S_1$  (thick line). Within the FO layer of finite thickness,  $L$ , the density of interacting particles gradually decreases and disappears once we reach the outside boundary,  $S_2$  (thin line), of the FO layer. This can be easily described if we consider two components of the matter, an interacting part plus a free part, thus

$$f(x, p) = f_i(x, p) + f_f(x, p), \quad (8)$$

which for conserved particles leads the following identity

$$N^\mu(x) = N_i^\mu(x) + N_f^\mu(x). \quad (9)$$

If there are no additional particle source or drain terms during the FO process, the conservation of the total particle number, eq. (7) with eq. (9), leads to

$$\partial_\mu N_i^\mu(x) = - \partial_\mu N_f^\mu(x). \quad (10)$$

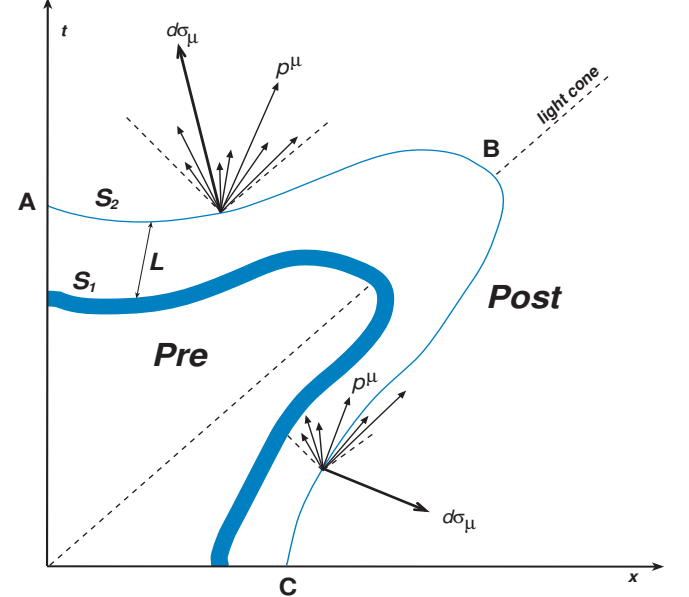


FIG. 1: Between A and B the surface is time-like, from B down to C it is space-like. The momentum of particles is  $p^\mu$ , the normal to the surface is  $d\sigma_\mu$ . Along the time-like region all particles emerging from a point belong to the Post FO side, while the particles originating from the space-like part of the FO surface divided between Pre and Post parts. Only those particles cross the surface which have their momentum on the post FO side and the FO surface.

Now, if we write the above equation, eq. (10), in terms

of the one particle distribution function, while keeping in mind that before freeze out ( $t < t_1, \mathbf{x} < \mathbf{x}_1$ ), the free component is still non-existent,  $f_f(t, \mathbf{x}, p) = 0$ , therefore

$$\frac{p^\mu}{p^0} \left[ \partial_\mu f_i(t, \mathbf{x}, p) \right] \equiv (\partial_t + \mathbf{v} \nabla) f_i(t, \mathbf{x}, p) = 0. \quad (11)$$

In an inhomogeneous system we may always introduce a characteristic length scale,  $\lambda'(x)$ , which at a given space point is associated with the inhomogeneity such as:

$$|\nabla f_i(x, p)| = f_i(x, p) \frac{1}{\lambda'(x)}, \quad (12)$$

where  $\lambda'(x)$  represents the typical range, over which the distribution function changes appreciably, see refs. [12, 13]. In an inhomogeneous system, this rate of spatial variation of the one-particle distribution function is related to the local gradients of density and temperature. Now, inserting the above identity into eq. (11), we get

$$\partial_t f_i(x, p) = -f_i(x, p) \frac{1}{\tau'(x)}, \quad (13)$$

where  $\tau' = \lambda'/|\mathbf{v}|$  is the characteristic time scale. The sign was chosen in a way that  $f_i$  decreases with time.

Furthermore, as time passes the number of interacting particles decreases with the same amount as the number of free particles is increasing. Thus, we find similar equations describing the evolution of the free component as eqs. (12, 13) only with opposite sign.

Before going further, we will write the above equations in a more general form, which can be used in both time-like and space-like cases

$$\frac{p^\mu}{p^0} \left[ \partial_\mu f_i(x, p) \right] \equiv \frac{1}{p^0} \underbrace{p^\nu d\sigma_\nu}_{\equiv p^s} \underbrace{d\sigma^\mu \partial_\mu}_{\equiv \partial_s} f_i(x, p), \quad (14)$$

where  $s$  is the coordinate axis in the direction of the FO normal vector,  $d\sigma_\mu$ , and we assumed that the change happens in the direction of  $d\sigma_\mu$  and it is negligible along the hypersurface of the front, see Appendix A.

Now, the above equation can be applied to any direction normal to the FO surface.<sup>1</sup> Thus, the kinetic equations describing the evolution of both the interacting and free components are

$$\begin{aligned} \partial_s f_i(x, p) ds &= -f_i(x, p) \frac{ds}{\lambda(s)}, \\ \partial_s f_f(x, p) ds &= +f_i(x, p) \frac{ds}{\lambda(s)}, \end{aligned} \quad (15)$$

<sup>1</sup>

	Time-like	Space-like
$\partial_s \equiv (d\sigma^\rho \partial_\rho)$	$\partial_t$	$\partial_x$
$p^s \equiv (p^\rho d\sigma_\rho)$	$p^0$	$p^x$
$s \equiv (x^\rho d\sigma_\rho)$	$t$	$x$
$\lambda(s)$	$\tau'(t)$	$\lambda'(x)$

where the characteristic mean length,  $\tilde{\lambda}(s)$  is either  $\lambda'(x)$ , or time,  $\tau'(t)$ , which governs the development.

The above form of the kinetic equations were used in recent works [6, 8, 9, 11] to model the FO process over a space-like layer, while the recent paper [10] for FO with a time-like normal vector.

However, the next step is to approximate the characteristic length,  $\tilde{\lambda}(s)$ , in the above equations. As in ref. [11], we are introducing a so called *escape probability*,

$$W_{esc} \equiv \tilde{\lambda}^{-1}(s), \quad (16)$$

such as this term describes the freeze out or the escape of particles from the interacting component into the free component. In a realistic case the FO probability may depend on the particle density and the momenta. Note that  $W_{esc}$  is a probability density !

A qualitative expression of the escape probability can be based on the simple assumption, that the particles with higher escape velocity component have a greater chance to freeze out. This assumption is expressing the momentum dependence of the FO probability. During the FO the interacting particles, which are closer to the outside boundary of the FO layer have a greater chance to freeze out, because the number of interacting particles is decreasing as the FO proceeds. Since the particles are crossing the FO surface only outwards in the direction of the FO normal vector, leads to a non-isotropic space-time dependent escape probability.

The above assumptions are generally valid for a FO description based on a the Boltzmann Transport Equation (BTE). In a realistic approach the FO is finished within a layer of finite thickness,  $L$ , which is approximately the length needed for a few collisions. However, we should not forget that generally we have three characteristic scales in a system governed by the kinetic equation, see [12, 13]. There is the correlation length,  $\lambda_c$  or duration of the collision  $\tau_c$ , followed by an average length or time between the collisions,  $\lambda$  or  $\tau$ , which are on microscopic scale, while on the macroscopic scale there is the hydrodynamical length,  $\lambda'$  or time  $\tau'$  scale. If the following conditions are satisfied:

$$\tau_c \ll \tau \ll \tau' \quad \text{or} \quad \lambda_c \ll \lambda \ll \lambda', \quad (17)$$

then we are in the Boltzmann kinetic regime. However, in different situations, such as high energy heavy ion collisions, there may exist extremely steep temperature and density gradients, i.e. shock waves, detonations, deflagrations. In the special case of freeze out the mean free path becomes very long, much longer than the initial system size. This simply means that we cannot have a complete FO in a finite layer of any thickness smooth enough to be modeled with the BTE. The proposed model, which overcomes the limitations of the BTE approach is the Modified Boltzmann Equation (MBTE), see ref. [14]. Unfortunately, it tends to a very complicated integro-differential equation. Therefore, since the FO description from the first principles is a very complex and time consuming task, it is very important to build a simplified,

but nontrivial model, which can help us understand the basic features of the freeze out process.

Now, we will give a schematic derivation of the escape probability based on the arguments made above. A more detailed treatment of the escape probability for FO in a finite layer was presented in ref. [11].

Let us follow a particle, starting from the inner surface of the FO layer,  $S_1$ , where  $x^\mu = 0$ . This particle is moving orthogonally outwards having the position,  $x^\mu$ , across the FO layer of finite length. The probability not-to-collide with anything on the way out depends on the number of particles and the remaining distance:

$$L - x^\mu d\sigma_\mu. \quad (18)$$

As this remaining distance becomes smaller the probability to freeze out becomes larger, thus, we may assume that the FO probability is inversely proportional to some power of this quantity [11].

Furthermore, if the particle momentum is not normal to the surface, the spatial distance increases further by  $\cos \theta_{\mathbf{p}} = p_x/|\mathbf{p}|$ , where  $\theta_{\mathbf{p}}$  is the angle between the FO normal vector,  $d\sigma$ , and  $\mathbf{p}$ . We can generalize this angular factor, as:

$$\cos \theta_{\mathbf{p}} \longrightarrow \left( \frac{p^\mu d\sigma_\mu}{p^\mu u_\mu} \right). \quad (19)$$

The detailed analysis of the covariant angular factor can be found in ref. [11, 15]. If the FO direction is in the time direction, i.e.  $d\sigma_\mu$  is time-like, and the particle momentum is also, (so that their scalar product  $p^\mu d\sigma_\mu$  is always positive) all particles fall into the forward light-cone, and all the momentum will be represented in the final FO spectra. Particularly, in the case when the FO normal vector is parallel to the flow velocity, the momentum dependent part of the escape probability or the angular factor is unity.

If we sum up the above assumptions we can approximate the probability for a particle to escape from a time-like layer as:

$$W_{esc}(x, p, d\sigma_\mu) = \frac{1}{\tau} \left( \frac{L}{L - x^\mu d\sigma_\mu} \right)^a \left( \frac{p^\mu d\sigma_\mu}{p^\mu u_\mu} \right)^a, \quad (20)$$

where the power,  $a$ , is influencing the freeze out profile across the layer.

Now, we can generalize the simple model presented in ref. [10] for the finite layer FO with a time-like normal vector following the above made arguments. We choose FO direction to be in the time-direction, thus, eq. (15) will lead to

$$\begin{aligned} \partial_t f_i &= -\frac{1}{\tau} \left( \frac{L}{L - t} \right) \left( \frac{p^\mu d\sigma_\mu}{p^\mu u_\mu} \right) f_i, \\ \partial_t f_f &= \frac{1}{\tau} \left( \frac{L}{L - t} \right) \left( \frac{p^\mu d\sigma_\mu}{p^\mu u_\mu} \right) f_i, \end{aligned} \quad (21)$$

where a simplified form of the Lorentz invariant escape probability eq. (20) with  $a = 1$  was used.

Solving the first equation we find that the interacting component deviates from the initial Jüttner shape,  $f_J(\mathbf{p})$ , as:

$$f_i = f_J(\mathbf{p}) \left( \frac{L - t}{L} \right)^{\frac{L}{\tau} \left( \frac{p^\mu d\sigma_\mu}{p^\mu u_\mu} \right)}. \quad (22)$$

Now, inserting the above result into the second differential equation from eq. (21), leads the momentum distribution of the frozen out particles,

$$\begin{aligned} f_f &= f_J(\mathbf{p}) - f_i \\ &= f_J(\mathbf{p}) \left[ 1 - \left( \frac{L - t}{L} \right)^{\frac{L}{\tau} \left( \frac{p^\mu d\sigma_\mu}{p^\mu u_\mu} \right)} \right] \xrightarrow{t \rightarrow L} f_J(\mathbf{p}). \end{aligned} \quad (23)$$

As  $t$  tends to the boundary of the FO layer, this distribution will tend to the original Jüttner distribution.

This is a highly unrealistic model, similar to the one resulting in the cut Jüttner distribution in Refs. [6, 8, 9] for the FO hypersurface with space-like normal vector. We can improve this model taking into account rescatterings in the interacting component in the same way as it was done in [10]. Adding an extra collision term into the description of an inhomogeneous system, will drive the evolution of the system to a state of local equilibrium, see [12, 13].

However, in the special case of FO, only the interacting term is maintaining some level of local equilibrium, thus:

$$\begin{aligned} \partial_t f_i &= -\frac{1}{\tau} \left( \frac{L}{L - t} \right) \left( \frac{p^\mu d\sigma_\mu}{p^\mu u_\mu} \right) f_i + \frac{1}{\tau_0} [f_{eq}(t) - f_i], \\ \partial_t f_f &= \frac{1}{\tau} \left( \frac{L}{L - t} \right) \left( \frac{p^\mu d\sigma_\mu}{p^\mu u_\mu} \right) f_i, \end{aligned} \quad (24)$$

where the interacting component approaches the equilibrated Jüttner distribution,  $f_{eq}$ , with  $\tau_0$  relaxation time.

Rethermalization within the interacting component happens simultaneously with the freeze out. This is the immediate rethermalization limit, a common simplification, that the local equilibrium is maintained at all times.

### A. Reference frames

Before going further, we need to define the possible reference frames, in which our calculations can be handled. Since, the properties of the matter are different on the two sides of the FO front, we may denote them as Pre and Post FO sides.

On the Pre FO side the matter is parameterized by an equilibrium distribution function. The frame where the matter is at rest, i.e.  $u^\mu = (1, 0, 0, 0)_{RFG}$ , is the local Rest Frame of the Gas, (RFG), see Fig. 2.

On the Post FO side, the frame which is attached to the freeze out front, i.e.  $d\sigma_\mu = (1, 0, 0, 0)_{RFF}$  for the time-like case, is the Rest Frame of the Front, (RFF).

Furthermore, there are a few important things to notice. If we are in the RFG frame, i.e.  $([t,x])$ , the flow velocity is always time-like, and  $u^\mu = (1, 0, 0, 0)_{RFG}$  in this system.

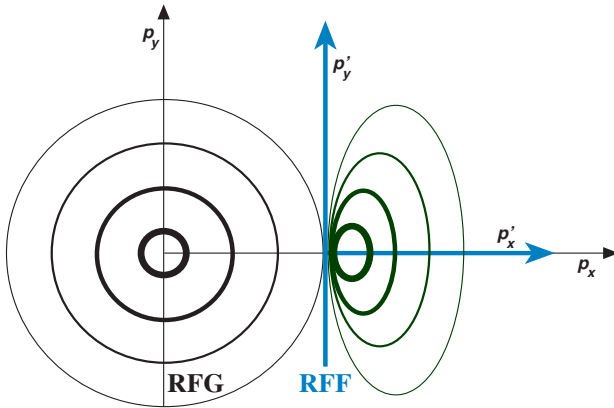


FIG. 2: The different reference frames, RFG and RFF as seen from the RFG, in momentum space. In RFG the initial equilibrium momentum distribution function is spherically symmetric, while in RFF the Post FO momentum distribution is depicted. In case of space-like FO the Post FO distribution function is continued on one hemisphere, as indicated in the figure. In the case of time-like FO the Post FO distribution extends to both hemispheres, but it is generally asymmetric, unless  $u_\mu$  and  $d\sigma_\mu$  are identical.

Now, if we take different characteristic points e.g. (A,B,C) on the FO hypersurface, then the value of the normal vector,  $d\sigma_\mu = (i, j, k, l)_{RFG}$ , is different at different points of the hypersurface in RFG.

A )  $d\sigma_\mu = (1, 0, 0, 0)_{RFG}$ , time-like

B )  $d\sigma_\mu = \gamma_\sigma(1, v_\sigma, 0, 0)_{RFG}$ .

C )  $d\sigma_\mu = \gamma_\sigma(1 + \epsilon, 1 - \epsilon, 0, 0)$ , where  $\epsilon \ll 1$ , just above the light-cone,

To calculate the parameters of the normal vector,  $d\sigma_\mu$ , for different cases listed above in the RFF, we simply make use of the Lorentz transformation. The normal vector of the time-like part of the freeze out hypersurface may be defined as the local  $t'$ -axis, while the normal vector of the space-like part may be defined as the local  $x'$ -axis. This defines the axes of the RFF, where Fig. 4 shows the RFF at point B. However, the four velocity in the RFG will be different in RFF,  $u^\mu = \gamma_\sigma(1, -v_\sigma, 0, 0)_{RFF}$ .

## B. Changes of the conserved current and energy-momentum tensor

The immediate rethermalization approach, i.e. assuming that  $\tau \gg \tau_0$ , will result in a Jüttner type of distribution for the interacting component. Therefore, the relaxation term in the above equation, eq. (24), can be

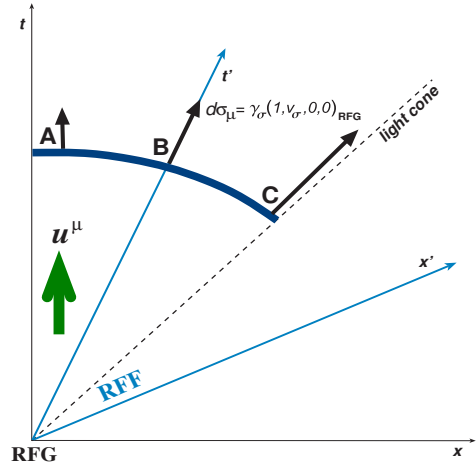


FIG. 3: A simple time-like FO-surface in the Rest Frame of the Gas (RFG:  $[t,x]$ ), where  $u^\mu = (1, 0, 0, 0)_{RFG}$ . The normal vectors of the FO front,  $d\sigma_\mu$ , are time-like and are plotted at three points: (A, B, C).

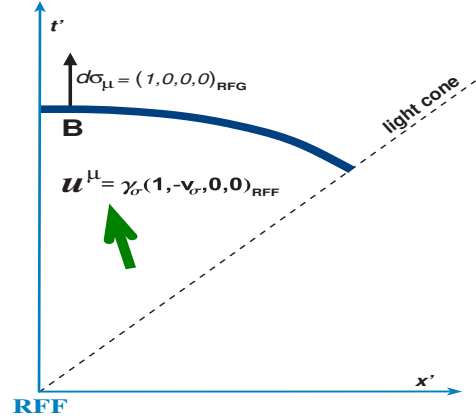


FIG. 4: The same time-like FO surface, which was depicted in Fig. 3 at point B in (RFF:  $[t',x']$ ), where  $d\sigma_\mu = (1, 0, 0, 0)_{RFF}$  and  $u^\mu = \gamma_\sigma(1, -v_\sigma, 0, 0)_{RFF}$ .

evaluated implicitly. Only its parameters,  $T(t)$ ,  $n(t)$  and  $u^\mu(t)$  need to be determined.

The change of conserved quantities caused by the particle transfer from the interacting matter into the free matter can be obtained in terms of distribution function of the interacting matter, eqs. (24). The new parameters of the distribution  $f_i$  after progressing by  $dt$  can be obtained from the change in the baryon four current as:

$$\begin{aligned} dN_i^\mu(t) &= dt \int \frac{d^3 p}{p^0} p^\mu \left[ \partial_t f_i \right] \\ &= -\frac{dt}{\tau} \left( \frac{L}{L-t} \right) \int \frac{d^3 p}{p^0} p^\mu \\ &\times \left[ \frac{p^0}{\gamma(p^0 - j^{\mu\nu} p_\nu \cos \theta_p)} \right] f_J(t, \mathbf{p}) \end{aligned} \quad (25)$$

and the change in the energy-momentum as:

$$\begin{aligned} dT_i^{\mu\nu}(t) &= dt \int \frac{d^3p}{p^0} p^\mu p^\nu \left[ \partial_t f_i \right] \\ &= -\frac{dt}{\tau} \left( \frac{L}{L-t} \right) \int \frac{d^3p}{p^0} p^\mu p^\nu \\ &\times \left[ \frac{p^0}{\gamma(p^0 - jup \cos \theta_{\mathbf{p}})} \right] f_J(t, \mathbf{p}), \end{aligned} \quad (26)$$

where the four-momentum of particles is  $p^\mu = (p^0, \mathbf{p})$ ,  $p = |\mathbf{p}|$ ,  $p^x = p \cos \theta_{\mathbf{p}}$ , the flow velocity of the interacting matter in RFF is  $u^\mu = \gamma(1, v, 0, 0)_{RFF}$ ,  $\gamma = \frac{1}{\sqrt{1-v^2}}$ ,  $u = |v|$  and  $j = \text{sign}(v)$ .

The general form for the change of conserved particle

density and energy density after a step  $dt$  are given in ref. [8, 9]:

$$dn_i(t) = u_i^\mu(t) dN_{i,\mu}(t), \quad (27)$$

$$de_i(t) = u_{\mu,i}(t) dT_i^{\mu\nu}(t) u_{\nu,i}(t). \quad (28)$$

While these equations are valid in any frame, we can calculate them in RFF, where the values of  $dN^\mu$  and  $dT^{\mu\nu}$  are given below.

The analytical results for the changes of the conserved current and energy-momentum tensor in the case of time-like FO are analogous to the calculations for the space-like FO layer, see ref. [11].

---


$$\begin{aligned} dN_i^0(t) &= -\frac{dt}{\tau} \left( \frac{L}{L-t} \right) \frac{n}{4ju\gamma} \left\{ -G_1^+(m) + G_1^-(m) \right\} \\ &\xrightarrow{m=0} -\frac{dt}{\tau} \left( \frac{L}{L-t} \right) n \left[ \frac{(3+v^2)}{3} \gamma^2 \right], \\ dN_i^x(t) &= \frac{dN_i^0(t)}{ju} - \frac{dt}{\tau} \left( \frac{L}{L-t} \right) \frac{n}{4ju\gamma} \left\{ -2b \left[ 2K_1(a) + aK_0(a) \right] \right\} \\ &\xrightarrow{m=0} -\frac{dt}{\tau} \left( \frac{L}{L-t} \right) n \left[ \frac{(3+v^2)}{3v} \gamma^2 - \frac{1}{v} \right], \end{aligned} \quad (29)$$

$$\begin{aligned} dT_i^{00}(t) &= -\frac{dt}{\tau} \left( \frac{L}{L-t} \right) \frac{nT}{4ju\gamma} \left\{ -G_2^+(m) + G_2^-(m) \right\} \\ &\xrightarrow{m=0} -\frac{dt}{\tau} \left( \frac{L}{L-t} \right) nT \left[ 3(1+v^2) \gamma^3 \right], \\ dT_i^{0x}(t) &= \frac{dT_i^{00}(t)}{ju} - \frac{dt}{\tau} \left( \frac{L}{L-t} \right) \frac{nT}{4ju\gamma} \left\{ -2b^2(3+u^2)K_2(a) - 2ab^2K_1(a) \right\} \\ &\xrightarrow{m=0} -\frac{dt}{\tau} \left( \frac{L}{L-t} \right) nT \left[ \frac{3(1+v^2) \gamma^3}{v} - \frac{\gamma(3+v^2)}{v} \right], \\ dT_i^{xx}(t) &= \frac{dT_i^{0x}(t)}{ju} - \frac{T}{\gamma ju} \left[ dN_i^x(t) - \frac{dN_i^0(t)}{ju} \right] \\ &- \frac{dt}{\tau} \left( \frac{L}{L-t} \right) \frac{nT}{4ju\gamma} \left\{ -\frac{2b^2}{ju}(1+3u^2)K_2(a) - 2juab^2K_1(a) \right\} \\ &\xrightarrow{m=0} -\frac{dt}{\tau} \left( \frac{L}{L-t} \right) nT \left[ \frac{3(1+v^2) \gamma^3}{v^2} - \frac{\gamma(3+v^2)}{v^2} + \frac{1}{\gamma v^2} - \frac{(1+3v^2)\gamma}{v^2} \right], \end{aligned}$$

$$\begin{aligned}
dT_i^{yy}(t) &= -\frac{dT_i^{xx}(t)}{2} - \frac{dt}{\tau} \left( \frac{L}{L-t} \right) \frac{nT}{8ju\gamma} \left\{ -G_3^+(m) + G_3^-(m) \right\} \\
&\xrightarrow{m=0} -\frac{dt}{\tau} \left( \frac{L}{L-t} \right) \frac{nT}{2} \left[ dT^{xx}(t) + dT^{00}(t) \right],
\end{aligned}$$

and

$$dT_i^{zz}(t) = dT_i^{yy}(t).$$

where,  $a = \frac{m}{T}$ ,  $b = a\gamma$  and  $n = 4\pi T^3 a^2 K_2(a) g_\pi \frac{e^{\mu/T}}{(2\pi\hbar)^3}$  is the particle density, while  $g_\pi = 3$  is the degeneracy factor for pions, and  $G_1^\pm(m)$ ,  $G_2^\pm(m)$ ,  $K_0(a)$ ,  $K_1(a)$ ,  $K_2(a)$  are defined in Appendix B. In the massless limit the particle density is,  $n = 8\pi T^3 g_\pi \frac{e^{\mu/T}}{(2\pi\hbar)^3}$ . The  $t$ -dependent factor,  $\frac{L}{L-t}$ , is just a multiplier in these calculations, and tends to unity if we are dealing with infinitely long FO, as in ref. [10, 11].

### III. RESULTS AND DISCUSSION

Now, we will present our results for the post FO distribution and the relevant quantities form this model, similarly to the way done in ref. [11]. The main aim of this work is to compare the finite FO layer results with the infinitely long FO description. All the results are calculated using the Lorentz invariant angular factor,  $\frac{p^\mu d\sigma_\mu}{p^\mu u_\mu}$ . The difference due to the Lorentz invariance of the angular factor compared with the simple,  $\cos\theta_p$ , angular factor is small. A brief review of this difference can be found in ref. [11].

We have used a simple EoS,  $e = \sigma_{SB} T^4$ , for a baryon-free massless gas, similarly to refs. [6, 8], and performed numerical calculations, where  $\sigma_{SB} = \frac{\pi^2}{10}$ . The change in Landau's flow velocity and the change of the temperature from eq. (28) results in a set of differential equations:

$$\begin{aligned}
d\ln T &= \frac{\gamma^2}{4\sigma_{SB} T^4} \left[ dT_i^{00} - 2vdT_i^{0x} + v^2 dT_i^{xx} \right], \quad (30) \\
dv &= \frac{3}{4\sigma_{SB} T^4} \left[ -vdT_i^{00} + (1+v^2)dT_i^{0x} - vdT_i^{xx} \right].
\end{aligned}$$

We will present our results for two different cases.

- I) The system is characterized by an infinitely long FO length, ( $t \rightarrow 100\lambda\tau$ ). The results are shown, on Figs. (5, 7, 8, 11, 12, 15, 18).
- F) The system is characterized by a finite FO layer, ( $L = 10\tau$ ). The results are shown, on Figs. (6, 9, 10, 13, 14, 16, 19).

The results for the two different cases I and F, listed above are presented in a systematic way on five set of figures.

#### 1. The evolution of temperature of the interacting component

The first set of figures, Figs. 5 and 6 shows the evolution of temperature of the interacting component in RFF.

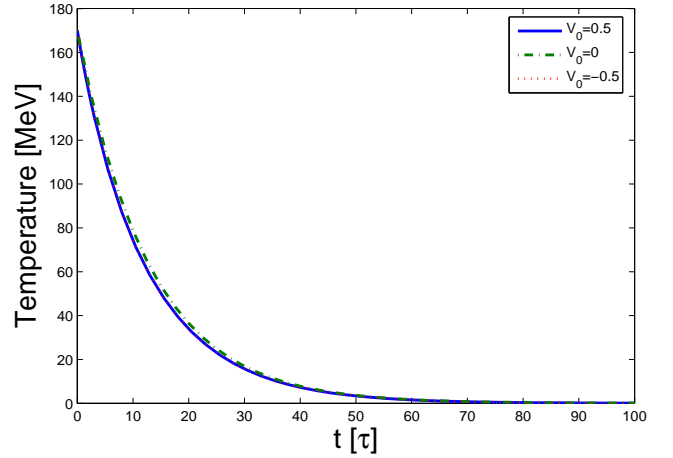


FIG. 5: The temperature of the interacting component in RFF, calculated for an infinitely long, ( $t \rightarrow 100\tau$ ), FO length. The initial temperature is  $T_0 = 170$  MeV, and the parameter,  $v_0$ , is the initial velocity. This corresponds to case I.

Comparing Fig. 5 with Fig. 6, we can see the difference between the finite and infinite FO. In the case of the finite FO layer, the freeze out is faster than in the case of an infinitely long FO description. The temperature curves belonging to different initial flow velocities but with opposite signs are the same. The matter with higher initial flow velocity,  $v_0$ , cools faster, but for small differences between the initial flow velocities, the resulting difference in the temperature is negligible. This is due to the fact that in the case of the time-like FO we do not apply any constraints on the momenta, i.e. the cut-off,  $\Theta(p^\mu d\sigma_\mu)$ . This can be seen, by comparing the temperature evolution here and in the space-like FO case, ref. [11].

The final FO temperature is zero, in both cases.

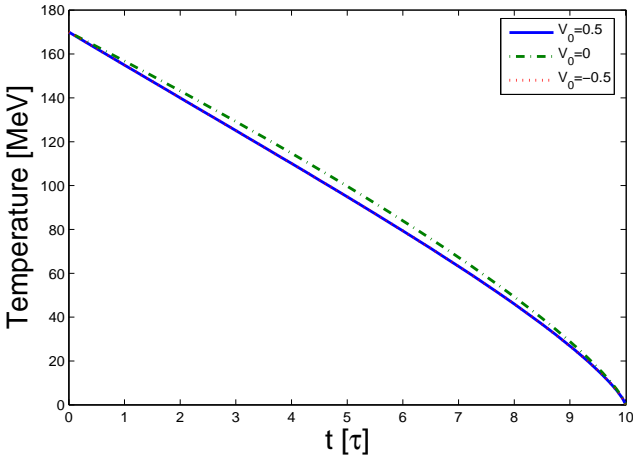


FIG. 6: The temperature of the interacting component in RFF, calculated for a finite ( $L = 10\tau$ ), FO layer. The initial temperature is  $T_0 = 170$  MeV, and the parameter,  $v_0$ , is the initial velocity. This corresponds to case F.

## 2. The evolution of common flow velocity of the interacting component in RFF and RFG

The second set of figures, Figs. 7, 8, and Figs. 9, 10 shows the evolution of the flow velocity in RFF and RFG respectively.

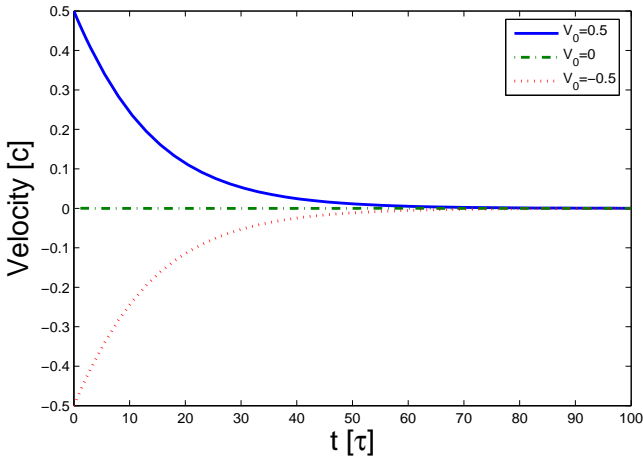


FIG. 7: The evolution of the flow velocity of the interacting component for a baryonfree massless gas, calculated for an infinitely long ( $t \rightarrow 100\tau$ ), FO length. The initial temperature is  $T_0 = 170$  MeV. The parameter,  $v_0$ , is the initial velocity, in RFF. This corresponds to case I.

First, comparing Fig. 7 with Fig. 9, we can see the difference between the finite and infinite FO description. In the case of the finite FO layer, velocity decrease is much faster than in the case of an infinitely long FO description.

Furthermore, comparing Fig. 7 with Fig. 8 or Fig. 9

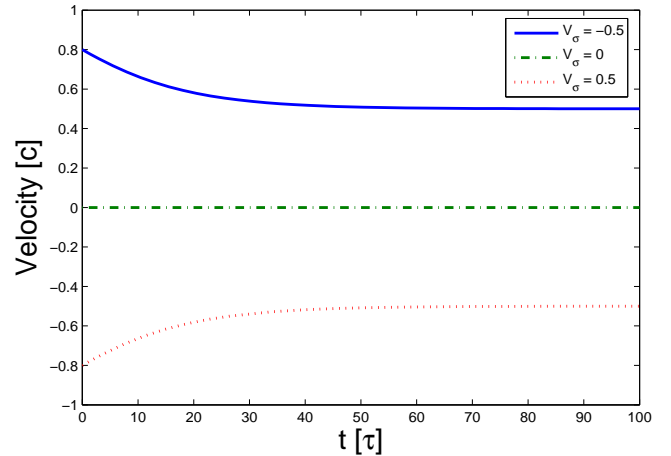


FIG. 8: The evolution of the flow velocity of the interacting component for a baryonfree massless gas, calculated for an infinitely long ( $t \rightarrow 100\tau$ ), FO length. The initial temperature is  $T_0 = 170$  MeV. The parameter,  $v_\sigma$ , is the initial flow velocity, in RFG. The flow parameter,  $v_\sigma$ , is in the direction of  $d\sigma_\mu$ , where  $d\sigma_\mu = \gamma_\sigma(1, -v_\sigma, 0, 0, 0)$ .

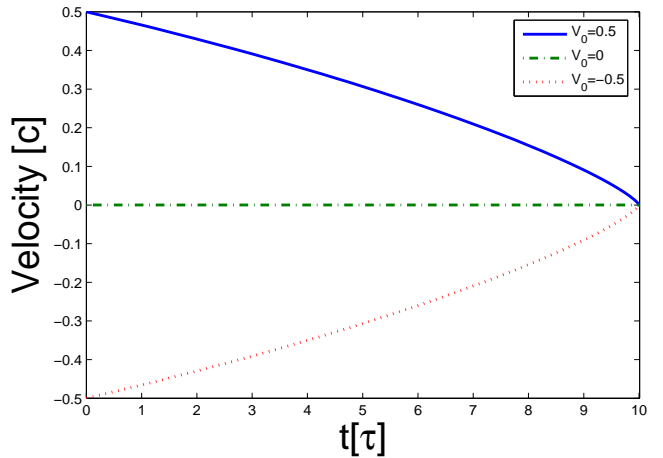


FIG. 9: The evolution of the flow velocity of the interacting component for a baryonfree massless gas, calculated for a finite ( $L = 10\tau$ ), FO length. The initial temperature is  $T_0 = 170$  MeV. The parameter,  $v_0$ , is the initial velocity, in RFF. This corresponds to case F.

with Fig. 10 we notice that in case of time-like FO the common flow velocity of interacting component tends to zero, while in case of space-like FO it tends to  $-1$ , (see ref. [11]). This is an artifact of the reference frame of the front, RFF, which behaves discontinuously at the light cone. In the rest frame of the gas, RFG, the change is continuous !

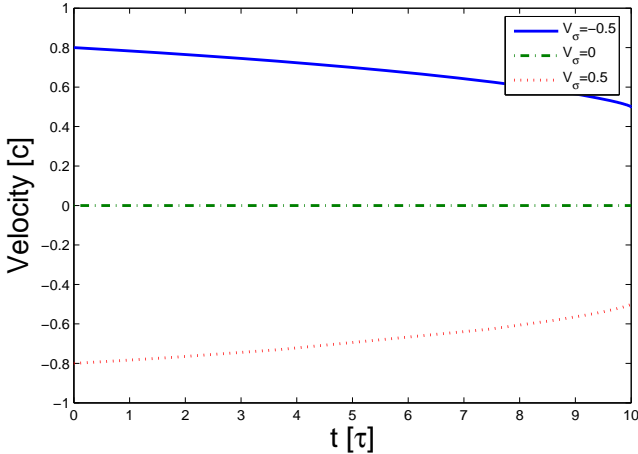


FIG. 10: The evolution of the flow velocity of the interacting component for a baryonfree massless gas, calculated for a finite ( $L = 10\tau$ ), FO length. The initial temperature is  $T_0 = 170$  MeV. The parameter,  $v_\sigma$ , is the initial flow velocity, in RFG. The flow parameter,  $v_\sigma$ , is in the direction of  $d\sigma_\mu$ , where  $d\sigma_\mu = \gamma_\sigma(1, -v_\sigma, 0, 0, 0)$ .

### 3. The transverse momentum and the contour plots of the post FO distribution

The third set of figures, Figs. (11, 12, 13, 14), shows the evolution of the local transverse momentum distribution and the corresponding contour plots of the post FO momentum distribution.

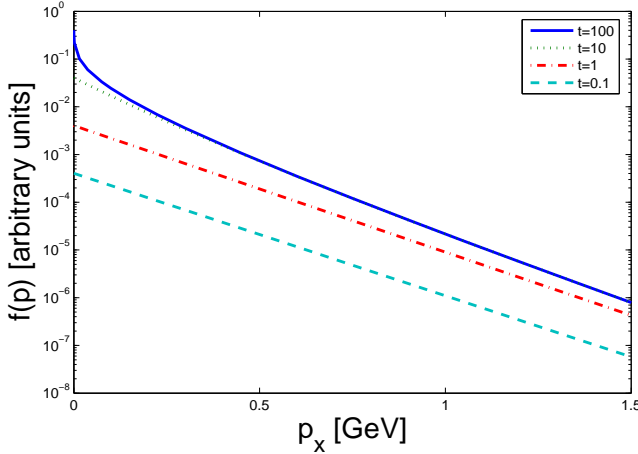


FIG. 11: The local transverse momentum (here  $p_x$ ) distribution for a baryonfree and massless gas at ( $p_y = 0$ ). The calculation was done for an infinitely long ( $t \rightarrow 100\tau$ ), FO length, where the initial flow velocity and temperature are,  $u^\mu = (1, 0, 0, 0)_{RFG}$ , and  $T_0 = 170$  MeV. The transverse momentum spectrum is obviously curved due to the freeze out process, particularly for low momenta.

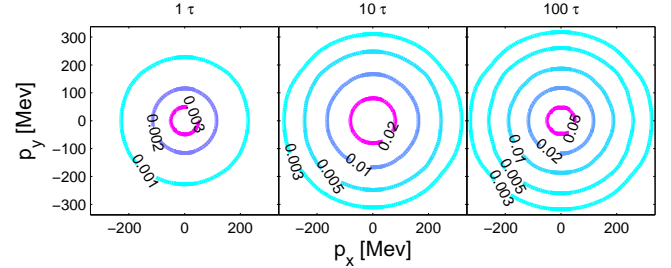


FIG. 12: The post FO distribution,  $f_{free}(x, \mathbf{p})$ , at point A of Fig. 3, for an infinitely long FO length. The figures correspond to different time points,  $t = 1\tau, 10\tau, 100\tau$  respectively. Contour lines are given at values represented on the figure. The initial flow velocity and temperature are,  $u^\mu = (1, 0, 0, 0)_{RFG}$  and  $T_0 = 170$  MeV. The maximum is increasing with  $t$  as indicated in Fig. 11.

We have presented a one-dimensional model here, but we assume that it is applicable for the direction transverse to the beam in heavy ion experiments. The plots presented should relate the transverse momentum distribution of measured particles.

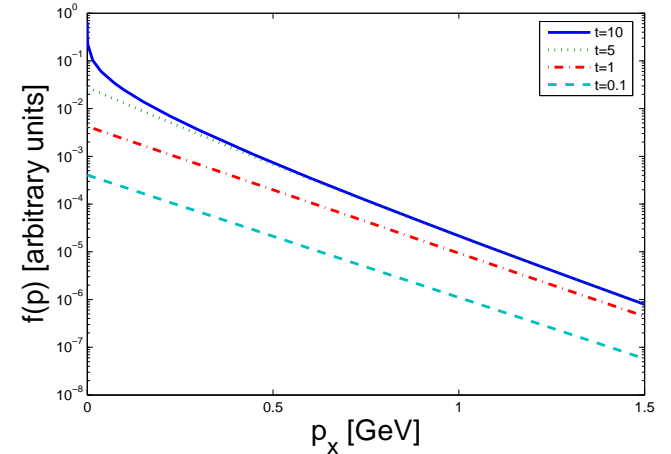


FIG. 13: The local transverse momentum (here  $p_x$ ) distribution for a baryonfree and massless gas at ( $p_y = 0$ ). The calculation was done for a finite ( $L = 10\tau$ ), FO length, where the initial flow velocity and temperature are,  $u^\mu = (1, 0, 0, 0)_{RFG}$ , and  $T_0 = 170$  MeV.

Now, comparing Figs. (11, 12) with Figs. (13, 14), we see that the post FO momentum distributions are qualitatively identical. The quantitative differences between the finite and infinite FO dynamics are small. The resulting post FO distribution are non-thermal distributions, they strongly deviate from exponential form in the low momentum region.

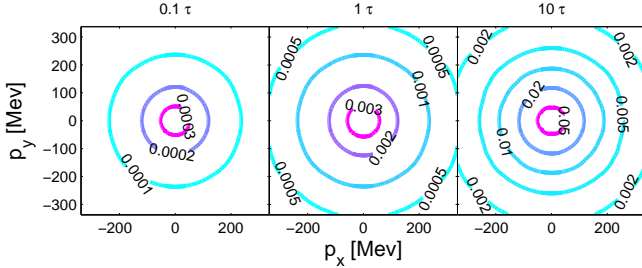


FIG. 14: The post FO distribution,  $f_{free}(x, \mathbf{p})$ , at point A of Fig. 3, for a finite FO length. The figures correspond to different time points,  $t = 0.1\tau, 1\tau, 10\tau$  respectively. Contour lines are given at values represented on the figure. The initial flow velocity and temperature are,  $u^\mu = (1, 0, 0, 0)_{RFG}$  and  $T_0 = 170$  MeV. The maximum is increasing with  $t$  as indicated in Fig. 13

#### 4. The slope of the transverse momentum distribution

The fourth set of figures, Figs. (15, 16), shows the evolution of the local transverse momentum distribution of different initial flow velocities.

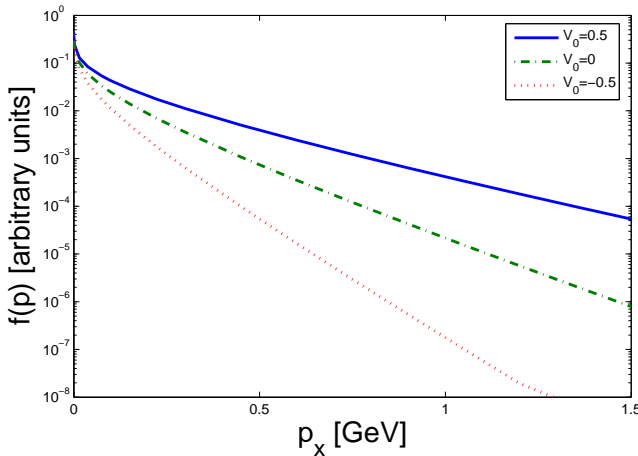


FIG. 15: The local transverse momentum distribution for a baryonfree and massless gas at ( $p_y = 0$ ). The calculation was done for an infinitely long, ( $t \rightarrow 100\tau$ ), FO length, where initial temperature is  $T_0 = 170$  MeV. The values of the initial flow velocity are  $u^\mu = (1, v, 0, 0)_{RFG}$ , where the values of  $v$  are represented on the figure. The transverse momentum spectrum is obviously curved due to the freeze out process, particularly for large initial flow velocities. The apparent slope parameter increase with increasing transverse momentum.

Comparing the two figures, Fig. 15 with Fig. 16, our conclusion is the same as in the previous section: the results do not change much if we switch the FO description from case I to case F.

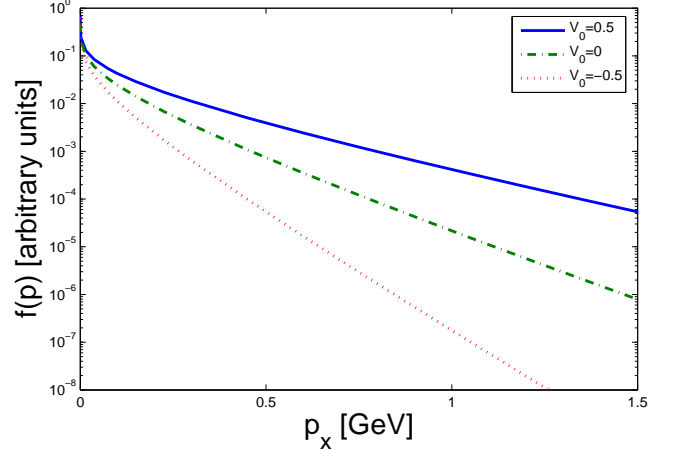


FIG. 16: The local transverse momentum distribution for a baryonfree and massless gas at ( $p_y = 0$ ). The calculation was done using the simple angular factor for a finite, ( $L = 10\tau$ ), FO layer, where the initial temperature is  $T_0 = 170$  MeV. The values of the initial flow velocity are represented on the figure.

#### 5. The boosted post FO distribution

The fifth set of figures Figs. (17) and Figs. (18, 19), shows the boosted Jüttner distribution and the final Post

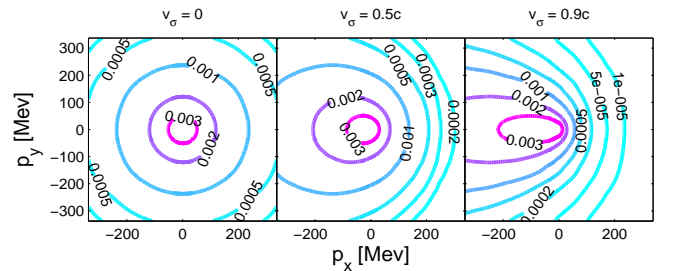


FIG. 17: The Jüttner distribution at point A and boosted to the frames at points B and C as depicted in Fig. 3, and presented in the RFF frames at those point respectively. The different figures correspond to different initial normal vectors,  $d\sigma^\mu = (1, v_\sigma, 0, 0)$ , where  $v_\sigma = 0, 0.5c, 0.9c$ . The initial temperature is  $T_0 = 170$  MeV. Contour lines are given at values presented in the figure. The distribution is asymmetric and elongated in the FO direction.

## IV. CONCLUSIONS

In this work we have presented a simple kinetic freeze out model for finite time-like layer. We have demonstrated that FO across a time-like surface in general leads

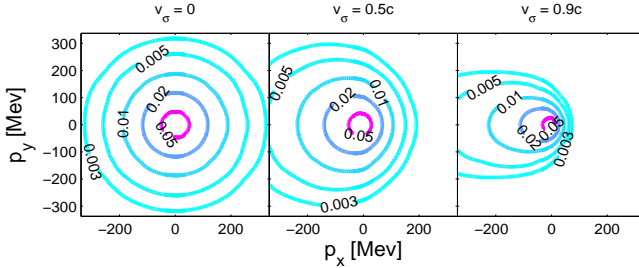


FIG. 18: The post FO distribution,  $f_{free}(x, \mathbf{p})$ , at points A, B, C of Fig. 3, in RFF, taken at infinity,  $t \rightarrow 100\tau$ . This is the same as the distribution at point A corresponding to different initial flow velocities,  $u^\mu = (1, -v_\sigma, 0, 0)$ , with  $v_\sigma = 0, 0.5c, 0.9c$  respectively and  $T_0 = 170$  MeV. Note that, while the post FO distribution is a Jüttner distribution at point A of Fig. 3, as  $(u^\mu = d\sigma^\mu)$ , the other two distributions are not boosted Jüttner distributions because  $(u^\mu \neq d\sigma^\mu)$ , see Fig. 17. The difference is that the post FO distribution is less elongated than the boosted Jüttner because it is a superposition

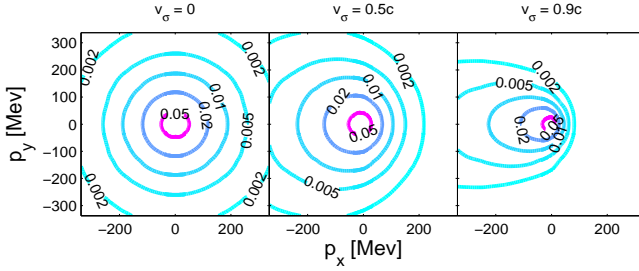


FIG. 19: The post FO distribution,  $f_{free}(x, \mathbf{p})$ , at points A, B, C of Fig. 3, in RFF, taken at finite  $L = 10\tau$ , FO length. This is the same as the distribution at point A corresponding to different initial flow velocities,  $u^\mu = (1, -v_\sigma, 0, 0)$ , with  $v_\sigma = 0, 0.5c, 0.9c$  respectively and  $T_0 = 170$  MeV. Note that, while the post FO distribution is a Jüttner distribution at point A of Fig. 3, as  $(u^\mu = d\sigma^\mu)$ , the other two distributions are not boosted Jüttner distributions because  $(u^\mu \neq d\sigma^\mu)$ , see Fig. 17. The difference is that the post FO distribution is less elongated than the boosted Jüttner, because it is a superposition of sources with decreasing speed in RFF as indicated in Fig. 9.

to non-equilibrated, anisotropic distribution. These distributions in general cannot be Lorentz transformed to a frame where the distribution is isotropic. The only exception is when the normal to the FO hypersurface is parallel to the local flow velocity. The usual practice of assuming the Jüttner distribution as a post FO distribution is in general not valid !

We can also see that while the boosted Jüttner distribution is elongated in the boost direction, i.e. in the direction of  $d\sigma_\mu$ , the post FO distribution is close to a spherical and isotropic distribution at low momenta and becomes elongated only at higher momenta, see Figs. 18 and 19. This special post FO distribution leads to a

curved " $p_\perp$  - spectrum". Here, we can also demonstrate (as in earlier works [8, 9]) that non-equilibrium processes in kinetic FO lead to observable effects.

We do not aim directly to apply the results presented here to experimental heavy ion collision data, instead our purpose was to study qualitatively the basic features of the freeze out effect, and to demonstrate the applicability of this covariant formulation for FO in a finite length.

We observe that the Jüttner distribution is not a good approximation for the post FO distribution just like in the case of a space-like FO. While in the case of space-like FO the Cancelling-Jüttner distribution introduced in ref. [16] is satisfactory.

Here in case of time-like FO this is not the case, and we will have to search for other simple approximations which can be applicable for a simple description of FO through a time-like surface.

## Acknowledgments

Some authors, L. P. Csérnai, A. Nyíri, K. Tamásius and E. Molnár, thanks the hospitality of the University of Cape-Town where parts of this work were done. E. M also thanks the hospitality of the Babeş-Bolyai University.

Enlightening discussions with Cs. Anderlik, S. Zscocke and T. S. Biró are gratefully acknowledged.

## APPENDIX A

Let us now consider the FO situation, where we have a directed process in a layer. The dominant change happens in the direction of the normal of the FO hypersurface,  $d\sigma^\mu$  (where  $d\sigma^\mu d\sigma_\mu = \pm 1$ ). We can decompose the 4-vector,  $p^\nu$  on the l.h.s. of the above equations into four orthogonal directions:

$$p^\nu = (p^\mu d\sigma_\mu) d\sigma^\nu + (p^\mu d\sigma_{1\mu}) d\sigma_1^\nu + (p^\mu d\sigma_{2\mu}) d\sigma_2^\nu + (p^\mu d\sigma_{3\mu}) d\sigma_3^\nu, \quad (A1)$$

where the 4-vectors,  $d\sigma_1^\nu$ ,  $d\sigma_2^\nu$ , and  $d\sigma_3^\nu$ , are tangent to the hypersurface and orthogonal to the normal,  $d\sigma^\nu$ . This leads to:

$$p^\nu \partial_\nu f(x, p) = [(p^\mu d\sigma_\mu) d\sigma^\nu + (p^\mu d\sigma_{1\mu}) d\sigma_1^\nu + (p^\mu d\sigma_{2\mu}) d\sigma_2^\nu + (p^\mu d\sigma_{3\mu}) d\sigma_3^\nu] \partial_\nu f(x, p), \quad (A2)$$

Now, we assume that the change happens in the direction of the normal and negligible along the hypersurface of the front, thus the last three terms can be neglected:

$$p^\nu \partial_\nu f(x, p) \approx (p^\mu d\sigma_\mu) d\sigma^\nu \partial_\nu f(x, p). \quad (A3)$$

## APPENDIX B

The definition of the modified Bessel function of the second kind,  $K_n(z)$ , is:

$$K_n(z) = \frac{2^n n!}{(2n)!} z^{-n} \int_z^\infty dx e^{-x} (x^2 - z^2)^{n-\frac{1}{2}}, \quad (\text{B1})$$

where  $n > -1$ . We make use of the following indefinite integral, see [17],

$$\int z^{\alpha-1} \Gamma(n, z) dz = \frac{z^\alpha \Gamma(n, z) - \Gamma(n + \alpha, z)}{\alpha}, \quad (\text{B2})$$

where the incomplete gamma function is defined as

$$\Gamma(n, z) = \int_z^\infty dt t^{n-1} e^{-t}. \quad (\text{B3})$$

The analytically not integrable functions  $G_n^-(m)$  and  $G_n^+(m)$  where, ( $n > -2$ ), are defined as:

$$\begin{aligned} G_n^\pm(m) &= \frac{1}{T^{n+2}} \int_0^\infty dp p \left( \sqrt{p^2 + m^2} \right)^n \\ &\times \Gamma\left(0, \frac{\gamma}{T} \sqrt{p^2 + m^2} \pm \frac{\gamma jup}{T}\right), \end{aligned} \quad (\text{B4})$$

furthermore, the massless limit leads to:

$$\begin{aligned} G_1^\pm(0) &= \frac{1}{T^3} \int_0^\infty dp p^2 \Gamma\left(0, \frac{\gamma}{T} p(1 \pm ju)\right) \\ &= \frac{2}{3\gamma^3} (1 \pm ju)^{-3}, \end{aligned} \quad (\text{B5})$$

$$\begin{aligned} G_2^\pm(0) &= \frac{1}{T^4} \int_0^\infty dp p^3 \Gamma\left(0, \frac{\gamma}{T} p(1 \pm ju)\right) \\ &= \frac{3}{2\gamma^4} (1 \pm ju)^{-4}. \end{aligned} \quad (\text{B6})$$

The general calculation of the integrals in RFF, is

$$\begin{aligned} &\int_0^\infty dp f(p) e^{-\frac{\gamma}{T}(\sqrt{p^2 + m^2} - jup)} \\ &= j\gamma T \int_b^a dz \left( u - \frac{z}{\sqrt{z^2 - a^2}} \right) e^{-z} \\ &\times f\left[\gamma T(juz - j\sqrt{z^2 - a^2})\right] \\ &+ j\gamma T \int_a^\infty dz \left( u + j\frac{z}{\sqrt{z^2 - a^2}} \right) e^{-z} \\ &\times f\left[\gamma T(juz + \sqrt{z^2 - a^2})\right], \end{aligned} \quad (\text{B7})$$

where,  $z = \gamma(\sqrt{p^2 + m^2} - jup)/T$ ,  $a = m/T$  and  $b = \gamma a$ .

---

[1] L. D. Landau, Izv. Akad. Nauk SSSR **17**, 51 (1953)  
[2] L. P. Csernai, Sov. JETP **65** (1987) 216; Zh. Eksp. Theor. Fiz. **92** (1987) 379.  
[3] F. Cooper and G. Frye, Phys. Rev. **D10** (1974) 186.  
[4] K. A. Bugaev, Nuclear Phys. A **606** (1996) 559.  
[5] L. P. Csernai, Zs. Lázár, D. Molnár, Heavy Ion Physics, **5** (1997) 467.  
[6] Cs. Anderlik, Zs. Lázár, V. K. Magas, L. P. Csernai, H. Stöcker and W. Greiner, Phys. Rev. C, **59** (1999) 388.  
[7] Cs. Anderlik, L. P. Csernai, F. Grassi, W. Greiner, Y. Hama, T. Kodama, Zs. Lázár, V. K. Magas, Phys. Rev. C, **59** (1999) 3309.  
[8] V. K. Magas, Cs. Anderlik, L. P. Csernai, F. Grassi, W. Greiner, Y. Hama, T. Kodama, Zs. Lázár and H. Stöcker, Heavy Ion Physics, **9** (1999) 193.  
[9] V. K. Magas, Cs. Anderlik, L. P. Csernai, F. Grassi, W. Greiner, Y. Hama, T. Kodama, Zs. Lázár and H. Stöcker, Phys. Lett. B, **459** (1999) 33; Nucl. Phys. **A661** (1999) 596.  
[10] V. K. Magas, A. Anderlik, Cs. Anderlik and L. P. Csernai, Eur. Phys. J. **C30** (2003) 255.  
[11] E. Molnár, L.P. Csernai, V.K. Magas, A. Nyíri and K. Tamosiunas, nucl-th/0503047.  
[12] R. Balescu, *Equilibrium and nonequilibrium statistical mechanics*, (Wiley and Sons, 1975).  
[13] R. Balescu, *Statistical Dynamics: Matter out of Equilibrium*, (Imperial College Press, 2000).  
[14] V.K. Magas, L.P. Csernai, V.K. Magas, E. Molnár, A. Nyíri and K. Tamosiunas Nucl. Phys. **A749** (2005) 202; L.P. Csernai, V.K. Magas, E. Molnár, A. Nyíri and K. Tamosiunas, hep-ph/0406082.  
[15] L. P. Csernai *et al.*, *Proceedings of the International Conference on Structure and Dynamics of Elementary Matter*, hep-ph/0401005.  
[16] K. Tamosiunas and L. P. Csernai, Eur. Phys. J. **A20** (2004) 269.  
[17] <http://functions.wolfram.com/>